HHS Public Access

Author manuscript

J Comp Neurol. Author manuscript; available in PMC 2019 December 01.

Published in final edited form as:

J Comp Neurol. 2018 December 01; 526(17): 2845–2855. doi:10.1002/cne.24530.

Alterations in synaptic density and myelination in response to exposure to high-energy charged particles

Dara L. Dickstein[1,2], **Ronan Talty**[2], **Erin Bresnahan**[2], **Merina Varghese**[2], **Bayley Perry**[1], **William G. M. Janssen**[2], **Allison Sowa**[2], **Erich Giedzinski**[3], **Lauren Apodaca**[3], **Janet Baulch**[3], **Munjal Acharya**[3], **Vipan Parihar**[3], and **Charles L. Limoli**[3]

[1]Uniformed Services University of Health Sciences, Bethesda, Maryland [2]Fishberg Department of Neuroscience, Icahn School of Medicine at Mount Sinai, New York, New York [3]Department of Radiation Oncology, University of California, Irvine, California

Abstract

High-energy charged particles are considered particularly hazardous components of the space radiation environment. Such particles include fully ionized energetic nuclei of helium, silicon, and oxygen, among others. Exposure to charged particles causes reactive oxygen species production, which has been shown to result in neuronal dysfunction and myelin degeneration. Here we demonstrate that mice exposed to high-energy charged particles exhibited alterations in dendritic spine density in the hippocampus, with a significant decrease of thin spines in mice exposed to helium, oxygen, and silicon, compared to sham-irradiated controls. Electron microscopy confirmed these findings and revealed a significant decrease in overall synapse density and in nonperforated synapse density, with helium and silicon exhibiting more detrimental effects than oxygen. Degeneration of myelin was also evident in exposed mice with significant changes in the percentage of myelinated axons and g-ratios. Our data demonstrate that exposure to all types of high-energy charged particles have a detrimental effect, with helium and silicon having more synaptotoxic effects than oxygen. These results have important implications for the integrity of the central nervous system and the cognitive health of astronauts after prolonged periods of space exploration.

Correspondence: Dara L. Dickstein, Department of Pathology, Uniformed Services University of the Health Sciences, Bethesda, MD 20814. dara.dickstein@usuhs.edu and Charles L. Limoli, Department of Radiation Oncology, University of California, Irvine, CA 92697-2695. climoli@uci.edu.

CONFLICT OF INTEREST

The authors declare they have no conflict of interest.

DISCLAIMER

The opinions expressed herein are those of the authors and are not necessarily representative of those of the government of the United States, the Uniformed Services University of the Health Sciences, the Department of Defense (DoD); or, the United States Army, Navy or Air Force.

COMPLIANCE WITH ETHICAL STANDARDS

RESEARCH INVOLVING ANIMALS

All procedures performed in studies involving animals were in accordance with the ethical standards of the institution or practice at which the studies were conducted.

INFORMED CONSENT

This article does not contain any studies with human participants performed by any of the authors.

Keywords

charged particles; dendritic spines; myelin; synapses

1 | INTRODUCTION

As NASA plans deep space travel of longer durations, the health consequences of exposure to the charged particles that permeate the cosmos have become of increasing concern. A mission to Mars and preparatory deep space gateway sorties inevitably result in exposure to high-energy protons derived from solar ejection events and the spectrum of charged particles ($Z \leq 26$) comprising the galactic cosmic rays (Nelson, 2016). Resultant exposures to these highly energetic particles can compromise tissue functionality due to the ionizations that result as they penetrate the hull of the spacecraft and traverse to the tissues of the body (Cucinotta, Alp, Sulzman, & Wang, 2014). Measurements of the radiation fields in deep space, and on the surface of Mars, have indicated that the accumulation of such particle traversal events are capable of exposing one to a total dose equivalent of ~ 1.0 sievert (Sv) over a mission to Mars approaching 900 days (Hassler et al., 2014; Zeitlin et al., 2013).

At present there is considerable uncertainty regarding the acute and chronic risks associated with deep space radiation exposure to the central nervous system (CNS), largely due to the fact that the majority of risk estimates have been derived from radiation-induced carcinogenesis (Cucinotta & Durante, 2006) and cataractogenesis (Blakely et al., 2010) and from radiation exposure in rapidly proliferating tissues (Measurement, 2006). This uncertainty is confounded by a wealth of recent data pointing to an unexpected sensitivity of the CNS to charged particle exposure (Parihar et al., 2015a; Parihar et al., 2016), dispelling long-standing, principally clinically-derived views, that labeled the CNS as a largely radioresistant organ (Tofilon & Fike, 2000). Emergent data from a variety of researchers have now shown that deep space relevant, low dose exposures possess the capability of disrupting neurotransmission at many levels, with implications for learning and memory, executive function, decision making, and fear extinction, leading to surprisingly persistent and adverse neurocognitive consequences spanning multiple regions of the brain (Britten et al., 2014; Britten et al., 2016; Davis, DeCicco-Skinner, & Hienz, 2015; Lonart et al., 2012; Parihar et al., 2015a; Parihar et al., 2016; Raber et al., 2016; Villasana, Rosenberg, & Raber, 2010). Such exposures may also impact mood disorders and may be capable of impacting social interactions, anxiety, and depression (Parihar et al., 2016; Yilmazer-Hanke, 2008). Suffice to say, partial manifestation of any subset of such radiation-induced aberrant behavior does not bode well for a team of astronauts working under/near complete autonomy for extended times, especially given the expectation to respond to a number of mission critical and/or unexpected scenarios.

In efforts to more completely understand the underlying biology responsible for charged particle effects in the irradiated brain, investigators have sought to link changes in cognition to alterations in the structural integrity of neurons. Early studies analyzing Golgi-impregnated brain sections found that dendritic complexity and spine density were reduced throughout hippocampal neurons in 5–6 month old mice following exposure (50 cGy) to

^{56}Fe ions (Allen, Raber, Chakraborti, Sharma, & Fike, 2015). Follow-up studies using similarly aged transgenic mice whose brains contained defined subsets of fluorescent neurons, revealed a remarkable sensitivity of hippocampal and prefrontal cortical neurons to proton, ^{16}O and ^{48}Ti ion exposure (Parihar et al., 2015a; Parihar et al., 2016; Parihar et al., 2015b). In these studies, space relevant doses (5–30 cGy) of charged particles significantly reduced dendritic complexity and spine density 6–24 weeks following irradiation, with a pronounced effect on immature spine morphologies (Parihar et al., 2015a; Parihar et al., 2016; Parihar et al., 2015b). Importantly, those animals exhibiting the largest drop in dendritic spine densities were found to exhibit the poorest performance on a behavioral task (Object in Place) known to interrogate the medial prefrontal circuit involved with spatial memory retention (Parihar et al., 2015a; Parihar et al., 2016). Other work linking charged particle exposures to altered neuronal morphology suggested the possibility that such structural alterations may underlie a certain fraction of the resultant neurocognitive complications (Kiffer et al., 2017; Raber et al., 2016).

The foregoing backdrop provides much of the rationale for undertaking the present studies, as progressively higher resolution confocal analyses have indicated that changes in dendritic arborization following charged particle exposure extend to major alterations in spine density and morphology. To further probe the ultrastructural consequences of charged particle exposure on neuronal integrity, confocal, and electron microscopic analyses were performed on tissue sections derived from mice irradiated at the age of 6 months. Here we report a detailed analysis of neuronal spine properties along *Cornu Ammonis* 1 (CA1) neurons of the hippocampus and the first systematic analyses of select neuronal parameters by electron microscopy, following exposure to charged particle irradiation typical of the deep space environment.

2 | METHODS

2.1 | Animals and charged particle irradiation

All animal procedures were carried out in accordance with National Institutes of Health and Institutional Animal Care guidelines and were approved by the Institutional Animal Care and Use Committee at the University of California, Irvine. Charged particles (^{16}Oxygen, ^{28}Silicon and ^{4}Helium) at 600 MeV/n were generated and delivered at the NASA Space Radiation Laboratory (NSRL) at Brookhaven National Laboratory at doses of 0 cGy or 30 cGy. The NSRL physics staff performed all dosimetry and confirmed spatial beam uniformity. For spine density quantification and classification, 6-month-old male transgenic mice [strain Tg(Thy1-EGFP) MJrsJ, RRID:IMSR JAX:007788, The Jackson Laboratory, Sacramento, CA] harboring the Thy1- EGFP transgene were used. Mice were bred and genotyped to confirm the presence of Thy1-EGFP transgene. For electron microscopy (EM) studies, 6-month-old male C57Bl/6 mice (RRID:IMSR JAX:000664) were used. For all experiments $n = 4–7$ animals per group were used. The numbers of animals used in each experiment are indicated in Table 1.

2.2 | Perfusion of mice

For confocal and spine analysis, all mice were perfused 6 weeks following irradiation as described previously (Parihar et al., 2015a; Parihar et al., 2016). For EM studies, at 6 weeks following irradiation mice were anesthetized with pentobarbital (50 mg/kg, intraperitoneal) and transcardially perfused with 1% paraformaldehyde (PFA) in phosphate buffered saline (PBS; pH 7.4) followed by 2% PFA/2% glutaraldehyde in PBS for 12 min, as described previously (Lazarczyk et al., 2016; Price et al., 2014; Steele et al., 2014b). The brains were removed and postfixed overnight at 4 °C in 2% PFA/2% glutaraldehyde in PBS. The brains were then sectioned on a Vibratome (Leica VT1000S, Leica Biosystems, Nussloch, Germany) at 250 μm thickness for EM. All sections were stored at 4 °C in PBS + 0.01% sodium azide until ready for use.

2.3 | Confocal microscopy

The expression of EGFP in specific subsets of neurons provides for high-resolution imaging and quantification of neuronal structure. Using an approach that precludes sampling bias of spines, EGFP labelled apical dendritic segments were selected with a systematic-random design in the CA1 *stratum radiatum* (SR) region of the hippocampus (Lazarczyk et al., 2016; Price et al., 2014; Steele et al., 2014a). Approximately 10 secondary or higher order branch apical dendritic segments/animal, 49–53 μm in length, were imaged on a Nikon Eclipse TE 2000-U microscope (Nikon, Japan) using a 60 ×/1.4 N.A. Plan-Apochromat objective with a digital zoom of 3.0 and an Ar/Kr laser at an excitation wavelength of 488 nm. All confocal stacks were acquired at 1024 × 1024 pixel resolution with a z-step of 0.1 μm and approximately 1 μm above and below the identified dendritic segment, a pinhole setting of one airy unit and optimal settings for gain and offset. In order for a dendritic segment to be optimally imaged the entire segment had to fall within a depth of 50 μm, dendritic segments had to be either parallel or at acute angles to the coronal surface of the section and had to be second order or higher (Lazarczyk et al., 2016; Price et al., 2014; Steele et al., 2014a). To improve voxel resolution and reduce optical aberration along the z-axis, the acquired images were deconvolved using an iterative blind deconvolution algorithm (AutoQuant X3 (version X3.0.1); MediaCybernetics, Rockville, MD).

2.4 | Spine analysis

After deconvolution, the confocal stacks were analyzed using Neurolucida 360 (MBF Bioscience) to examine global and local morphometric characteristics of dendritic spines, such as density, shape (stubby, mushroom, and thin), and head diameter. This software allows for automated digitization and reconstructions of 3D neuronal and spine morphology from multiple confocal stacks on a spatial scale and averts the subjective errors encountered during manual tracing (Dickstein et al., 2016). Neurolucida 360 also classifies spines into thin, mushroom, or stubby and measures spine head diameter and surface area. Spines were labeled thin or mushroom if the ratio of their maximum head diameter to maximum neck diameter was >1.1. Spines that fit those criteria and had a maximum head diameter of <0.40 μm were classified as thin spines, otherwise they were classified as mushroom spines. Spines that did not exhibit a neck were classified as stubby. Spine reconstruction and quantification were done using Neurolucida 360 automatic analysis followed by manual inspection and

correction. All analyses were performed by a single person who was blinded to the treatment groups.

2.5 | Electron microscopy

Coronal sections (250 μm-thick) encompassing the CA1 region of the hippocampus were prepared for EM as reported previously (Lazarczyk et al., 2016; Price et al., 2014; Steele et al., 2014a). The slices were cryoprotected in graded phosphate buffer/glycerol washes at 4 °C and manually microdissected to obtain blocks containing the CA1 region. The blocks were rapidly freeze-plunged into liquid propane cooled by liquid nitrogen (−190 °C) in a universal cryofixation system KF80 (Reichert-Jung, Leica Microsystems, Wetzlar, Germany) and subsequently immersed in 1.5% uranyl acetate dissolved in anhydrous methanol at −90 °C for 24 hr in a cryosubstitution unit (Leica). Block temperatures were raised from −90 to −45 °C in steps of 4 °C per hour, blocks were washed with anhydrous methanol, and infiltrated with Lowicryl resin (Electron Microscopy Sciences) at −45 °C. The resin was polymerized by exposure to ultraviolet light (360 nm) for 48 hr at −45 °C followed by 24 hr at 0 °C. Block faces were trimmed and ultrathin sections (90 nm) were cut with a diamond knife (Diatome) on an ultramicrotome (Reichert-Jung) and at least 10 serial sections were collected on formvar/carbon-coated nickel slot grids (Electron Microscopy Sciences, Hatfield, PA).

2.6 | Quantitative analysis of synapse density

For synapse quantification, serial section micrographs were imaged at 15,000× on a Hitachi H-7000 transmission electron microscope using an AMT Advantage CCD camera (Advanced Microscopy Techniques, Woburn, MA). Given that we only focused on apical dendritic spines, we analyzed synapses located in the SR of the hippocampal CA1 field (Figure 1a). An unbiased stereological approach using the physical disector was performed to measure CA1 SR synapse density, as described in our previous work and in reports by others (Hara et al., 2011; Hara et al., 2012; Lazarczyk et al., 2016; Price et al., 2014; Steele et al., 2014a). The physical disector approach samples objects in proportion to their number, independent of size, shape, or orientation of the postsynaptic densities (PSDs). Here, an unbiased counting frame was randomly superimposed over the EM micrograph and only synapses within the counting frame and that did not violate the counting frame rules were counted (Mouton, 2002). Nine sets of serial images across the same set of five consecutive ultrathin sections (Figure 1b,c) were taken for each animal and imported into Adobe Photoshop (version CC 2018 19.1.2, Adobe Systems, San Jose, CA). All axospinous synapses were identified within the first two and the last two images of each five-section serial set, and counted if they were contained in the reference image but not in the corresponding look-up image. To increase sampling efficiency, the reference image and look-up image were then reversed; thus each animal included in the current study contributed synapse density data from a total of 18 disector pairs (Figure 1d). The total volume examined was 11.317 μm^3, and the height of the disector was 180 nm and synapse density was calculated per μm^3. Axospinous synapse density was calculated as the total number of unique counted synapses from both images divided by the total volume of the disector (area × height of disector). The criteria for inclusion as an axospinous synapse included the presence of a presynaptic terminal and a distinct PSD separated by a clear

synaptic cleft. The same volume was sampled for each group. In addition to total synapse density, we also measured the densities of nonperforated and perforated synapses. Perforated synapses were defined by the presence of a discontinuity in the PSD. A single person, blinded to each of the treatment groups, performed all analyses.

2.7 | Quantitative analysis of myelination

To characterize the degree of myelination, the numbers of myelinated and unmyelinated axons were counted in 12 randomly selected, nonoverlapping fields of the hippocampal sulcus from each animal. Single sections were imaged at 10,000 × on a Hitachi H-7000 transmission electron microscope using an AMT (Advanced Microscopy Techniques, Woburn, MA) Advantage CCD camera. Both the number of myelinated axons per square millimeter and the percent of total myelinated axons were calculated. On average, 1,184 total axons were counted per animal. An additional six randomly selected, nonoverlapping images were taken per animal at 15,000 × to evaluate myelin sheath thickness through g-ratio analysis. Four measurements were recorded for each myelinated axon: the longest axon diameter, the shortest axon diameter, the longest myelin width, and the shortest myelin width. To calculate the g-ratio, the average diameter for each axon was divided by the average axon diameter plus twice the average myelin width (Dupree, Polak, Hensley, Pelligrino, & Feinstein, 2015; Murcia-Belmonte et al., 2016). Myelin regions that exhibited fixation artifacts or noncompaction were excluded from the analysis. On average, the g-ratios of 93 myelinated axons were analyzed per animal. A single person, blinded to the treatment groups, performed all analyses.

2.8 | Statistical analysis

One-way ANOVAs with Bonferroni's post hoc tests were used to test for significance when comparing data from control and irradiated mice for synapse density, percent myelinated axons, axonal diameter, myelin sheath thickness, and g-ratios. The α level was set at 0.05 with values of $p < 0.05$ considered statistically significant. All data were represented as mean ± SEM. All statistical analyses were carried out using Prism software (GraphPad Software).

3 | RESULTS

3.1 | Charged particle exposure induces deficits in spontaneous exploration

Our past work has shown that animals exposed to energetic charged particles of varying mass exhibited significant impairments on behavioral tasks known to interrogate the integrity of hippocampal and cortical circuitry (Acharya et al., 2017; Parihar et al., 2015a; Parihar et al., 2016; Parihar et al., 2018). These studies assessed the functional consequences of various charged particle exposures on the brain 6 weeks after exposure to the same charged particles used here (i.e., ^{16}O, ^{28}Si, and ^{4}He) using a variety of open field behavioral tasks (Novel Object recognition, NOR; Object In Place, OIP; and Temporal Order, TO) known to be dependent (albeit not exclusively) on intact perirhinal cortex (PRC), medial prefrontal cortex (mPFC) and hippocampal function (Barker, Bird, Alexander, & Warburton, 2007; Barker & Warburton, 2011). For such tasks, functionally intact mice exhibit a preference toward novel objects or those that have been moved to a novel location, whereas

mice exposed to charged particles showed lower preference for novel objects or newly positioned objects as compared to controls (Figure 2, adapted from Acharya et al., 2017; Parihar et al., 2015b; Parihar et al., 2016; Parihar et al., 2018).

3.2 | Charged particle exposure affects spine density and structure

Dendritic spine density as well as spine morphology influences synaptic function and changes in spine size can play a substantial role in mediating cognitive function (Harris & Stevens, 1989). Our previous studies where mice were irradiated with either ^{16}O or ^{48}Ti particles showed a significant and persistent reduction in the total number of dendritic spines in the mPFC (Parihar et al., 2015b; Parihar et al., 2016). In the present study, we assessed spine density in the CA1 SR region of the hippocampus. We analyzed a total of 24,349 spines from apical dendrites (Table 1). Figure 3a depicts a representative image of dendritic segments from each group. One way-ANOVA analysis revealed significant decrease in the total spine density in the irradiated mice ($F_{[3,14]} = 4.728$, $p = 0.018$), with post hoc analysis revealing a significant difference between controls and ^{4}He mice (Figure 3b).

Next, we examined if charged particle irradiation can affect specific spine types (thin, mushroom, and stubby). The various spine types are proposed to have unique roles in mediating cognitive function, complementing their distinctive morphology. Thin spines are thought to be more immature and “plastic” and are linked to learning as they contain a predominantly greater number of the N-methyl-D-aspartate (NMDA) glutamate receptors, whereas mushroom spines may represent more stable “mature”, functionally stronger, “memory” spines as they contain more 2-amino-3-(3-hydroxy-5-methyl-isoxazol-4-yl)propanoic acid (AMPA) receptors (Harris & Stevens, 1989; Murthy, Schikorski, Stevens, & Zhu, 2001; Tackenberg, Ghori, & Brandt, 2009). In regards to stubby spines, their function is still unclear. Some argue that stubby spines are “immature” plastic spines and are predominantly found during development but can persist into adulthood (Benavides-Piccione, Ballesteros-Yanez, DeFelipe, & Yuste, 2002; Bourne & Harris, 2007). Others theorize stubby spines are a more stable spine and may be transitional structures that will enlarge, possibly to mushroom spines (reviewed in Kanjhan, Noakes, & Bellingham, 2016). Given the varying function of different spine types, we assessed whether charged particle irradiation can affect spine shape. We found that there was a significant decrease in the density of thin spines in all irradiated mice compared to controls ($F_{[3,14]} = 7.704$, $p = 0.003$; Figure 3c). We also found significant changes in stubby spine density with an increase in the density of spines in the ^{16}O exposed group compared to controls, ^{28}Si, and ^{4}He, ($F_{[3,14]} = 16.68$, $p < 0.0001$; Figure 3d). Similar results were observed in mushroom spine density with ^{16}O exposed mice having significantly more mushroom spines than the control and the ^{4}He groups and an increasing trend compared with the ^{28}Si group ($F_{[3,14]} = 9.405$, $p = 0.0012$; Figure 3e). We also examined head diameter in all spines. Our analysis revealed a significant increase in total spine head diameter in ^{16}O and ^{28}Si exposed mice compared to controls and the ^{4}He group ($F_{[3,14]} = 19.28$, $p < 0.0001$; Figure 4a). When we examined the different spine types we found similar results, with ^{28}Si exposed groups having larger thin spines ($F_{[3,14]} = 8.692$, $p = 0.0017$; Figure 4b), and ^{16}O exposed mice having larger stubby ($F_{[3,14]} = 6.822$, $p = 0.0046$; Figure 4c), and mushroom spines ($F_{[3,14]} = 13.19$, $p = 0.0002$; Figure 4d).

3.3 | Charged particle irradiation results in a decrease in synapse density

Having found that charged particle irradiation affects the density and size of the various spine types, we subsequently examined its impact on synapses and synapse morphology at the ultrastructural level using quantitative EM. We examined synapses on spines from the SR dendritic domain of the hippocampal CA1 region and quantified total synapse density as well as the density of perforated and nonperforated synapses. Approximately 13,178 synapses were assessed (approximately 600 synapses per animal) across serial EM sections using the disector method (Table 1; see Figure 1 for steps in disector method). Analysis of the density of synapses from SR revealed a significant decrease in total synapse density in ^{4}He, ^{16}O, and ^{28}Si irradiated mice compared to nonirradiated control mice and in ^{16}O irradiated mice compared to ^{4}He mice ($F_{[3,17]} = 20.23$, $p < 0.0001$; Figure 5a). Further analysis of synapse type revealed a significant decrease in density of nonperforated synapses in ^{4}He and ^{28}Si irradiated mice ($F_{[3,17]} = 19.52$, $p < 0.0001$) but not ^{16}O irradiated mice compared to controls (Figure 5b). ^{4}He mice had lower nonperforated synapse density compared to ^{16}O irradiated mice. Although trends toward decreased perforated synapses in irradiated cohorts were noted ($F_{[3,17]} = 2.989$, $p < 0.0602$), no significant difference was observed in the density of perforated synapses in any of the irradiated groups compared to control mice (Figure 5c).

3.4 | Charged particle exposure results in a decrease of myelinated axons

To determine whether myelin density and myelin structure were compromised in irradiated mice, we examined axon myelination and structure in the hippocampal formation by EM. Representative images of myelinated and nonmyelinated axons from the different experimental groups can be seen (Figure 6a). Approximately 26,051 axons were counted (1,184 axons per animal on average) across serial EM sections using the disector method (Table 1). We found a significant decrease in the percentage of myelinated axons relative to controls in the hilus of ^{16}O, ^{28}Si, and ^{4}He irradiated mice compared to controls ($F_{[3,17]} = 5.217$, $p = 0.01$; Figure 6b). In addition to the number of myelinated axons, we also performed morphometric analysis of myelination of axons and calculated g-ratios (the ratio of axon diameter to fiber diameter) for each group. Comparison of g-ratios demonstrated significant differences between groups ($F_{[3,1818]} = 31.24$, $p < 0.0001$; Figure 6c). Interestingly, the smallest caliber axons, < 0.4 μm, in ^{16}O and ^{28}Si irradiated mice and 0.4 μm–0.6 μm diameter in the ^{16}O irradiated mice ($F_{[3,486]} = 5.217$, $p = 0.01$), showed a decrease in g-ratio compared to controls, whereas axons larger than 0.6 μm diameter did not exhibit any differences between groups (Figure 6d). The thinnest axons also were more affected in ^{16}O irradiated mice compared to the other irradiated groups (Figure 6d).

4 | DISCUSSION

Much of what we know concerning the response of the CNS to ionizing radiation exposure comes from the clinical literature, where cranial radiotherapy is used routinely to forestall malignant progression in the brain (Makale, McDonald, Hattangadi-Gluth, & Kesari, 2017). This has also fostered some unfortunate misconceptions regarding the response of the brain to cosmic radiation exposure, where the radiation types and microdosimetric properties are vastly different, and the doses and dose rates are orders of magnitude lower (Cucinotta et al.,

2014; Nelson, 2016). These realities portend very different biological responses, where dose response relationships are not linear, and where the majority of neurocognitive complications resulting from charged particle exposure transpire in the relative (or near complete) absence of cell loss. To reconcile discrepancies between cell loss and cognitive decline, we have focused on determining whether radiation-induced alterations in dendritic complexity, spine and synapse density, and myelination and/or morphologic plasticity might elicit more subtle disruptions to network connectivity capable of impairing neurotransmission.

Here we show that charged particle irradiation is capable of altering dendritic spine densities in the CA1 of the hippocampus, with the most significant impact on the more immature thin spines, corroborating our past findings in the mPFC using similar (Parihar et al., 2015a; Parihar et al., 2016) or in the dentate gyrus using different radiation modalities and/or post-irradiation time points (Parihar & Limoli, 2013; Parihar et al., 2015b). As the predominant spine morphology in the mature brain (Harris & Stevens, 1989), thin spines are largely decorated with NMDA receptors that exhibit reduced sensitivity to glutamate than AMPA receptors. Thin spines exhibit elevated temporal plasticity as they seek out new synaptic connections (Attardo, Fitzgerald, & Schnitzer, 2015; Berry & Nedivi, 2017), and the capability of charged particle exposures to reduce these structures relative to more mature spine types, suggests that short-term rather than long-term processes of learning and memory are preferentially impacted (Bloss et al., 2013). Related data derived from us and others using behavioral tests to interrogate cognitive tasks mediated by the hippocampus and the mPFC support that contention (Britten et al., 2014; Lonart et al., 2012; Parihar et al., 2015a; Parihar et al., 2016), and are corroborated from nonspace radiation studies, finding that selective changes in spine number and morphology in the prefrontal cortex can be associated with functional impairments in cognition (Bloss, Morrison, Hof, & Dickstein, 2011). These and other data (Allen et al., 2015; Raber et al., 2016) have clearly demonstrated that low doses of cosmic radiation can elicit persistent and marked cognitive decline and serve to further dispel the idea that neurocognitive sequelae need not be linked to the attrition of neuronal or other cell types in the brain, but can be the result of more subtle changes at the subcellular, synaptic level.

We also noted an increase in the density and head diameter of mushroom and stubby spines following ^{16}O irradiation. While the causes of this remain uncertain, such a change could be a compensatory mechanism to counteract the detrimental effects of radiation and preserve memory function. It has been suggested that spine structure is tightly correlated to synaptic strength and studies have shown that there is a positive correlation between the spine head volume, the PSD area, the presynaptic active zone area, and the number of AMPA-type glutamate receptors (Harris & Stevens, 1989; Matsuzaki et al., 2001; Takumi, Ramirez-Leon, Laake, Rinvik, & Ottersen, 1999). Mushroom spines typically have synapses with larger PSDs and have been proposed to enhance synaptic efficacy by increasing the surface area for receptor activation. An increase in PSD length could result in an increase in glutamate receptor content and enhance synaptic efficacy (Geinisman, 2000; Jones & Harris, 1995). Given the uncertain function of stubby spines, it is difficult to ascertain what the observed changes in response to radiation means functionally. Important too is the realization that morphologic plasticity of select spine types is not general throughout the

brain but rather distinct between select regions (Attardo et al., 2015; Bloss et al., 2011; Bloss et al., 2013). Indeed, our previous studies in the dentate gyrus did not find a change in spine volume and showed time-dependent worsening of spine density using a different irradiation method (Parihar & Limoli, 2013; Parihar et al., 2015b). This confounds attempts to generalize data collected along CA1 neurons at a single point in time, as radiation-induced changes in hippocampal function may not necessarily translate to other cortical regions implicated in learning and memory (Attardo et al., 2015; Bloss et al., 2011; Bloss et al., 2013).

The idea that spines are morphological surrogates for excitatory synapses has been largely based on EM data showing that the majority of such synapses are located on spines rather than the dendritic shaft (Berry & Nedivi, 2017). Here we report the first detailed analysis of charged particle-induced changes in synapse density and myelination by EM. Our data reveals that exposure to any of the three charged particle species caused significant drops in overall synapse density, with the primary effect on the nonperforated versus perforated synapses in the CA1. It is possible that the reduction of nonperforated synapses, which are normally located on thin spines, renders the CNS unable to make new synaptic connections and decreases the learning capabilities of the CNS (Bourne & Harris, 2007; Kasai et al., 2010). Certain studies have found age-related decrements in spatial and working memory to correlate with reductions in perforated synapses (Geinisman, de Toledo-Morrell, & Morrell, 1986a, 1986b; Hara et al., 2012), but the functional significance of radiation-induced reductions in nonperforated versus perforated synapses remains uncertain.

Myelin is a major component of white matter and it has been established that white matter tracts are highly vulnerable to damage from injury (Mierzwa, Marion, Sullivan, McDaniel, & Armstrong, 2015), stress (Csabai, Wiborg, & Czeh, 2018; Liu, Dietz, Hodes, Russo, & Casaccia, 2018) and in various neurodegenerative diseases (Wang et al., 2018). As the electrically insulating, protective sheath maintaining conduction velocity throughout the CNS, alterations in the myelin sheath, such as distribution, length and thickness, have significant potential for disrupting short- and long-range neurotransmission (Micu, Plemel, Caprariello, Nave, & Stys, 2018). Reduced myelination in the hippocampus, detected using histochemical or immunohistochemical techniques, was associated with decreased object recognition memory in a rat model of schizophrenia (Wischhof, Irrsack, Osorio, & Koch, 2015) and impaired cognition in a rat model of hypoxia-induced ischemia (Huang, Liu, Cheung, & Chen, 2009). Our analysis of the hippocampal sulcus by EM revealed a significant decrease in the percentage of myelinated axons following exposure to the charged particles used in this study. Given the low doses used, it is unlikely that depletion of oligoprogenitors would be responsible for reduced myelination, although direct myelin damage, radiation-induced disruptions to myelin production and/or perturbations to axo-myelinic signalling could account for the observed changes (Micu et al., 2018). In other models of neurodegenerative disorders, such as Alzheimer’s disease, the 5×FAD mouse showed higher g-ratio that resulted from a combination of thinner myelin and thinner axon calibre in the hippocampal CA1 (Gu et al., 2018), whereas the APP/PS1 mouse showed lower g-ratio, with thicker myelin sheaths and smaller internode length than the wild-type control (Wu et al., 2017). Our data demonstrated that irradiated animals had lower g-ratios; whether this may be due to thicker myelin, shrinkage of axons relative to the myelin sheath,

or reduced internode length in response to injury would need to be further examined. Collectively, EM analysis has uncovered for the first time, specific ultrastructural changes to neurons caused by charged particle irradiation, and points to the potential of the space radiation environment to perturb global circuitry, through subtle yet significant reductions in synapse density and myelination.

Here we report the impact of a single low dose of three separate charged particles on a number of ultrastructural features of neurons. Mice approximating the age of astronauts were irradiated and evaluated 6 weeks following acute exposure for changes in spines, synapses, and myelination. Dendrites, dendritic spines, and synapses serve critical roles in neurotransmission, helping in the formation and shaping of circuit connectivity throughout the brain before and after a variety of insults. Precisely how cosmic radiation exposure impacts the temporal and morphologic plasticity of spines and synapses and how such an evolving landscape influences learning and memory, remain a challenge in the field of space radiobiology and neuroscience. Given the global and random nature of radiation exposure in space, cause and effect become more difficult to assess and the outcomes for the CNS more difficult to predict. Despite the inherent uncertainties associated with such damage, the changes documented here point to an increased likelihood of global circuit disruption and increased risk of manifesting aberrant behavior during deep space travel. Further work will need to identify how specific circuits can be protected to mitigate the acute and chronic risks to the CNS associated with deep space radiation exposure.

ACKNOWLEDGMENTS

This work was supported by National Aeronautics and Space Administration NSCOR grant NNX15AI22G (C.L.L.). We would like to thank the members of the Dickstein and Limoli laboratories for technical assistance and discussion, and the Microscopy CoRE at the Icahn School of Medicine at Mount Sinai.

Funding information

NASA, Grant/Award Number: NNX15AI22G

REFERENCES

Acharya MM, Baddour AA, Kawashita T, Allen BD, Syage AR, Nguyen TH, … Baulch JE (2017). Epigenetic determinants of space radiation-induced cognitive dysfunction. Scientific Reports, 7, 42885 10.1038/srep42885 [PubMed: 28220892]

Allen AR, Raber J, Chakraborti A, Sharma S, & Fike JR (2015). (56) Fe irradiation alters spine density and dendritic complexity in the mouse hippocampus. Radiation Research, 184(6), 586–594. 10.1667/RR14103.1 [PubMed: 26579941]

Attardo A, Fitzgerald JE, & Schnitzer MJ (2015). Impermanence of dendritic spines in live adult CA1 hippocampus. Nature, 523(7562), 592–596. 10.1038/nature14467 [PubMed: 26098371]

Barker GR, Bird F, Alexander V, & Warburton EC (2007). Recognition memory for objects, place, and temporal order: A disconnection analysis of the role of the medial prefrontal cortex and perirhinal cortex. The Journal of Neuroscience, 27(11), 2948–2957. 10.1523/JNEUROSCI.5289-06.2007 [PubMed: 17360918]

Barker GR, & Warburton EC (2011). When is the hippocampus involved in recognition memory? The Journal of Neuroscience, 31(29), 10721–10731. 10.1523/JNEUROSCI.6413-10.2011 [PubMed: 21775615]

Benavides-Piccione R, Ballesteros-Yanez I, DeFelipe J, & Yuste R (2002). Cortical area and species differences in dendritic spine morphology. Journal of Neurocytology, 31(3–5), 337–346. [PubMed: 12815251]

Berry KP, & Nedivi E (2017). Spine dynamics: Are they all the same? Neuron, 96(1), 43–55. 10.1016/j.neuron.2017.08.008 [PubMed: 28957675]

Blakely EA, Kleiman NJ, Neriishi K, Chodick G, Chylack LT, Cucinotta FA, … Shore RE (2010). Radiation cataractogenesis: Epidemiology and biology. Radiation Research, 173(5), 709–717. 10.1667/RRXX19.1 [PubMed: 20426671]

Bloss E, Morrison J, Hof P, & Dickstein D (2011). Influence of aging and neurodegenration on dendritic spine morphology. Translational Neurosceince, 2(1), 49–60.

Bloss EB, Puri R, Yuk F, Punsoni M, Hara Y, Janssen WG, … Morrison JH (2013). Morphological and molecular changes in aging rat prelimbic prefrontal cortical synapses. Neurobiology of Aging, 34(1), 200–210. 10.1016/j.neurobiolaging.2012.05.014 [PubMed: 22727942]

Bourne J, & Harris KM (2007). Do thin spines learn to be mushroom spines that remember? Current Opinion in Neurobiology, 17(3), 381–386. 10.1016/j.conb.2007.04.009 [PubMed: 17498943]

Britten RA, Davis LK, Jewell JS, Miller VD, Hadley MM, Sanford LD, … Lonart G (2014). Exposure to mission relevant doses of 1 GeV/nucleon (56)Fe particles leads to impairment of attentional set-shifting performance in socially mature rats. Radiation Research, 182(3), 292–298. 10.1667/RR3766.1 [PubMed: 25029107]

Britten RA, Jewell JS, Miller VD, Davis LK, Hadley MM, & Wyrobek AJ (2016). Impaired spatial memory performance in adult Wistar rats exposed to low (5–20 cGy) doses of 1 GeV/n (56)Fe particles. Radiation Research, 185(3), 332–337. 10.1667/RR14120.1 [PubMed: 26943453]

Csabai D, Wiborg O, & Czeh B (2018). Reduced synapse and axon numbers in the prefrontal cortex of rats subjected to a chronic stress model for depression. Frontiers in Cellular Neuroscience, 12, 24 10.3389/fncel.2018.00024 [PubMed: 29440995]

Cucinotta F, Alp M, Sulzman F, & Wang M (2014). Space radiation risks to the central nervous system. Life Sceinces in Space Research, 2, 54–69.

Cucinotta FA, & Durante M (2006). Cancer risk from exposure to galactic cosmic rays: Implications for space exploration by human beings. The Lancet Oncology, 7(5), 431–435. 10.1016/S14702045(06)70695-7 [PubMed: 16648048]

Davis CM, DeCicco-Skinner KL, & Hienz RD (2015). Deficits in sustained attention and changes in dopaminergic protein levels following exposure to proton radiation are related to basal dopaminergic function. PLoS One, 10(12), e0144556 10.1371/journal.pone.0144556 [PubMed: 26658810]

Dickstein DL, Dickstein DR, Janssen WG, Hof PR, Glaser JR, Rodriguez A, … Tappan SJ (2016). Automatic dendritic spine quantification from confocal data with Neurolucida 360. Current Protocols in Neuroscience, 77, 1.27.1–1.27.21. 10.1002/cpns.16 [PubMed: 27696360]

Dupree JL, Polak PE, Hensley K, Pelligrino D, & Feinstein DL (2015). Lanthionine ketimine ester provides benefit in a mouse model of multiple sclerosis. Journal of Neurochemistry, 134(2), 302–314. 10.1111/jnc.13114 [PubMed: 25846048]

Geinisman Y (2000). Structural synaptic modifications associated with hippocampal LTP and behavioral learning. Cerebral Cortex, 10(10), 952–962. [PubMed: 11007546]

Geinisman Y, de Toledo-Morrell L, & Morrell F (1986a). Aged rats need a preserved complement of perforated axospinous synapses per hippocampal neuron to maintain good spatial memory. Brain Research, 398(2), 266–275. [PubMed: 3801904]

Geinisman Y, de Toledo-Morrell L, & Morrell F (1986b). Loss of perforated synapses in the dentate gyrus: Morphological substrate of memory deficit in aged rats. Proceedings of the National Academy of Sciences of the United States of America, 83(9), 3027–3031. [PubMed: 3458260]

Gu L, Wu D, Tang X, Qi X, Li X, Bai F, … Zhang Z (2018). Myelin changes at the early stage of 5XFAD mice. Brain Research Bulletin, 137, 285–293. 10.1016/j.brainresbull.2017.12.013 [PubMed: 29288735]

Hara Y, Park CS, Janssen WG, Punsoni M, Rapp PR, & Morrison JH (2011). Synaptic characteristics of dentate gyrus axonal boutons and their relationships with aging, menopause, and memory in

female rhesus monkeys. The Journal of Neuroscience, 31(21), 7737–7744. 10.1523/JNEUROSCI.0822-11.2011 [PubMed: 21613486]

Hara Y, Park CS, Janssen WG, Roberts MT, Morrison JH, & Rapp PR (2012). Synaptic correlates of memory and menopause in the hippocampal dentate gyrus in Rhesus monkeys. Neurobiology of Aging, 33(2), 421 e417–421 e428. 10.1016/j.neurobiolaging.2010.09.014

Hara Y, Punsoni M, Yuk F, Park CS, Janssen WG, Rapp PR, & Morrison JH (2012). Synaptic distributions of GluA2 and PKMzeta in the monkey dentate gyrus and their relationships with aging and memory. The Journal of Neuroscience, 32(21), 7336–7344. 10.1523/JNEUROSCI.0605-12.2012 [PubMed: 22623679]

Harris KM, & Stevens JK (1989). Dendritic spines of CA 1 pyramidal cells in the rat hippocampus: Serial electron microscopy with reference to their biophysical characteristics. The Journal of Neuroscience, 9(8), 2982–2997. [PubMed: 2769375]

Hassler DM, Zeitlin C, Wimmer-Schweingruber RF, Ehresmann B, Rafkin S, Eigenbrode JL, … Team, M. S. L. S. (2014). Mars' surface radiation environment measured with the Mars science Laboratory's curiosity rover. Science, 343(6169), 1244797 10.1126/science.1244797 [PubMed: 24324275]

Huang Z, Liu J, Cheung PY, & Chen C (2009). Long-term cognitive impairment and myelination deficiency in a rat model of perinatal hypoxic-ischemic brain injury. Brain Research, 1301, 100–109. 10.1016/j.brainres.2009.09.006 [PubMed: 19747899]

Jones DG, & Harris RJ (1995). An analysis of contemporary morphological concepts of synaptic remodelling in the CNS: Perforated synapses revisited. Reviews in the Neurosciences, 6(3), 177–219. [PubMed: 8717635]

Kanjhan R, Noakes PG, & Bellingham MC (2016). Emerging roles of filopodia and dendritic spines in motoneuron plasticity during development and disease. Neural Plasticity, 2016, 3423267 10.1155/2016/3423267 [PubMed: 26843990]

Kasai H, Hayama T, Ishikawa M, Watanabe S, Yagishita S, & Noguchi J (2010). Learning rules and persistence of dendritic spines. The European Journal of Neuroscience, 32(2), 241–249. 10.1111/j.1460-9568.2010.07344.x [PubMed: 20646057]

Kiffer F, Carr H, Groves T, Anderson JE, Alexander T, Wang J, … Allen AR (2017). Effects of (1)H + (16)O charged particle irradiation on short-term memory and hippocampal physiology in a murine model. Radiation Research, 189, 53–63. 10.1667/RR14843.1 [PubMed: 29136391]

Lazarczyk MJ, Kemmler JE, Eyford BA, Short JA, Varghese M, Sowa A, … Dickstein DL (2016). Major histocompatibility complex class I proteins are critical for maintaining neuronal structural complexity in the aging brain. Scientific Reports, 6, 26199 10.1038/srep26199 [PubMed: 27229916]

Liu J, Dietz K, Hodes GE, Russo SJ, & Casaccia P (2018). Wide-spread transcriptional alternations in oligodendrocytes in the adult mouse brain following chronic stress. Developmental Neurobiology, 78(2), 152–162. 10.1002/dneu.22533 [PubMed: 28884925]

Lonart G, Parris B, Johnson AM, Miles S, Sanford LD, Singletary SJ, & Britten RA (2012). Executive function in rats is impaired by low (20 cGy) doses of 1 GeV/u (56)Fe particles. Radiation Research, 178(4), 289–294. [PubMed: 22880624]

Makale MT, McDonald CR, Hattangadi-Gluth JA, & Kesari S (2017). Mechanisms of radiotherapy-associated cognitive disability in patients with brain tumours. Nature Reviews. Neurology, 13(1), 52–64. 10.1038/nrneurol.2016.185 [PubMed: 27982041]

Matsuzaki M, Ellis-Davies GC, Nemoto T, Miyashita Y, Iino M, & Kasai H (2001). Dendritic spine geometry is critical for AMPA receptor expression in hippocampal CA1 pyramidal neurons. Nature Neuroscience, 4(11), 1086–1092. 10.1038/nn736 [PubMed: 11687814]

Micu I, Plemel JR, Caprariello AV, Nave KA, & Stys PK (2018). Axo-myelinic neurotransmission: A novel mode of cell signalling in the central nervous system. Nature Reviews. Neuroscience, 19(1), 49–58. 10.1038/nrn.2017.128 [PubMed: 29118449]

Mierzwa AJ, Marion CM, Sullivan GM, McDaniel DP, & Armstrong RC (2015). Components of myelin damage and repair in the progression of white matter pathology after mild traumatic brain injury. Journal of Neuropathology and Experimental Neurology, 74(3), 218–232. 10.1097/NEN.0000000000000165 [PubMed: 25668562]

Mouton PR (2002). Principles and practices of unbiased stereology. Baltimore: The Johns Hopkins University Press.

Murcia-Belmonte V, Esteban PF, Martinez-Hernandez J, Gruart A, Lujan R, Delgado-Garcia JM, & de Castro F (2016). Anosmin-1 over-expression regulates oligodendrocyte precursor cell proliferation, migration and myelin sheath thickness. Brain Structure & Function, 221(3), 1365–1385. 10.1007/s00429-014-0977-4 [PubMed: 25662897]

Murthy VN, Schikorski T, Stevens CF, & Zhu Y (2001). Inactivity produces increases in neurotransmitter release and synapse size. Neuron, 32(4), 673–682. [PubMed: 11719207]

National Council on Radiation Protection and Measurements. (2006). Information needed to make radiation protection recommendations for space missions beyond low-earth orbit/recommendations of the National Council on Radiation Protection and Measurements. Bethesda, MD: National Council on Radiation Protection and Measurements.

Nelson GA (2016). Space radiation and human exposures, a primer. Radiation Research, 185(4), 349–358. [PubMed: 27018778]

Parihar VK, Allen B, Tran KK, Macaraeg TG, Chu EM, Kwok SF, … Limoli CL (2015a). What happens to your brain on the way to Mars. Science Advances, 1(4), e1400256 10.1126/sciadv.1400256 [PubMed: 26180843]

Parihar VK, Pasha J, Tran KK, Craver BM, Acharya MM, & Limoli CL (2015b). Persistent changes in neuronal structure and synaptic plasticity caused by proton irradiation. Brain Structure & Function, 220(2), 1161–1171. 10.1007/s00429-0140709-9 [PubMed: 24446074]

Parihar VK, Allen BD, Caressi C, Kwok S, Chu E, Tran KK, … Limoli CL (2016). Cosmic radiation exposure and persistent cognitive dysfunction. Scientific Reports, 6, 34774 10.1038/srep34774 [PubMed: 27721383]

Parihar VK, & Limoli CL (2013). Cranial irradiation compromises neuronal architecture in the hippocampus. Proceedings of the National Academy of Sciences of the United States of America, 110(31), 12822–12827. 10.1073/pnas.1307301110 [PubMed: 23858442]

Parihar VK, Maroso M, Syage A, Allen BD, Angulo MC, Soltesz I, & Limoli CL (2018). Persistent nature of alterations in cognition and neuronal circuit excitability after exposure to simulated cosmic radiation in mice. Experimental Neurology, 305, 44–55. 10.1016/j.expneurol.2018.03.009 [PubMed: 29540322]

Price KA, Varghese M, Sowa A, Yuk F, Brautigam H, Ehrlich ME, & Dickstein DL (2014). Altered synaptic structure in the hippocampus in a mouse model of Alzheimer's disease with soluble amyloid-beta oligomers and no plaque pathology. Molecular Neurodegeneration, 9, 41 10.1186/1750-1326-9-41 [PubMed: 25312309]

Raber J, Allen AR, Weber S, Chakraborti A, Sharma S, & Fike JR (2016). Effect of behavioral testing on spine density of basal dendrites in the CA1 region of the hippocampus modulated by (56)Fe irradiation. Behavioural Brain Research, 302, 263–268. 10.1016/j.bbr.2016.01.035 [PubMed: 26801826]

Steele J, Brautigam H, Short J, Sowa A, Shi M, Yadav A, … Disckstein D (2014a). Early fear memory defects are associated with altered synaptic plasticity and molecular architecture in the TgCRND8 Alzheimer's mouse model. The Journal of Comparative Neurology, 522, 2319–2335. [PubMed: 24415002]

Steele JW, Brautigam H, Short JA, Sowa A, Shi M, Yadav A, … Dickstein DL (2014b). Early fear memory defects are associated with altered synaptic plasticity and molecular architecture in the TgCRND8 Alzheimer's disease mouse model. The Journal of Comparative Neurology, 522(10), 2319–2335. 10.1002/cne.23536 [PubMed: 24415002]

Tackenberg C, Ghori A, & Brandt R (2009). Thin, stubby or mushroom: Spine pathology in Alzheimer's disease. Current Alzheimer Research, 6(3), 261–268. [PubMed: 19519307]

Takumi Y, Ramirez-Leon V, Laake P, Rinvik E, & Ottersen OP (1999). Different modes of expression of AMPA and NMDA receptors in hippocampal synapses. Nature Neuroscience, 2(7), 618–624. 10.1038/10172 [PubMed: 10409387]

Tofilon PJ, & Fike JR (2000). The radioresponse of the central nervous system: A dynamic process. Radiation Research, 153(4), 357–370. [PubMed: 10798963]

Villasana L, Rosenberg J, & Raber J (2010). Sex-dependent effects of 56Fe irradiation on contextual fear conditioning in C57BL/6J mice. Hippocampus, 20(1), 19–23. 10.1002/hipo.20659 [PubMed: 19489001]

Wang SS, Zhang Z, Zhu TB, Chu SF, He WB, & Chen NH (2018). Myelin injury in the central nervous system and Alzheimer's disease. Brain Research Bulletin, 140, 162–168. 10.1016/j.brainresbull.2018.05.003 [PubMed: 29730417]

Wischhof L, Irrsack E, Osorio C, & Koch M (2015). Prenatal LPS-exposure–a neurodevelopmental rat model of schizophrenia–differentially affects cognitive functions, myelination and parvalbumin expression in male and female offspring. Progress in Neuro-Psychopharmacology & Biological Psychiatry, 57, 17–30. 10.1016/j.pnpbp.2014.10.004 [PubMed: 25455585]

Wu Y, Ma Y, Liu Z, Geng Q, Chen Z, & Zhang Y (2017). Alterations of myelin morphology and oligodendrocyte development in early stage of Alzheimer's disease mouse model. Neuroscience Letters, 642, 102–106. 10.1016/j.neulet.2017.02.007 [PubMed: 28174059]

Yilmazer-Hanke DM (2008). Morphological correlates of emotional and cognitive behaviour: Insights from studies on inbred and outbred rodent strains and their crosses. Behavioural Pharmacology, 19(5–6), 403–434. 10.1097/FBP.0b013e32830dc0de [PubMed: 18690101]

Zeitlin C, Hassler DM, Cucinotta FA, Ehresmann B, Wimmer-Schweingruber RF, Brinza DE, … Reitz G (2013). Measurements of energetic particle radiation in transit to Mars on the Mars science laboratory. Science, 340(6136), 1080–1084. 10.1126/science.1235989 [PubMed: 23723233]

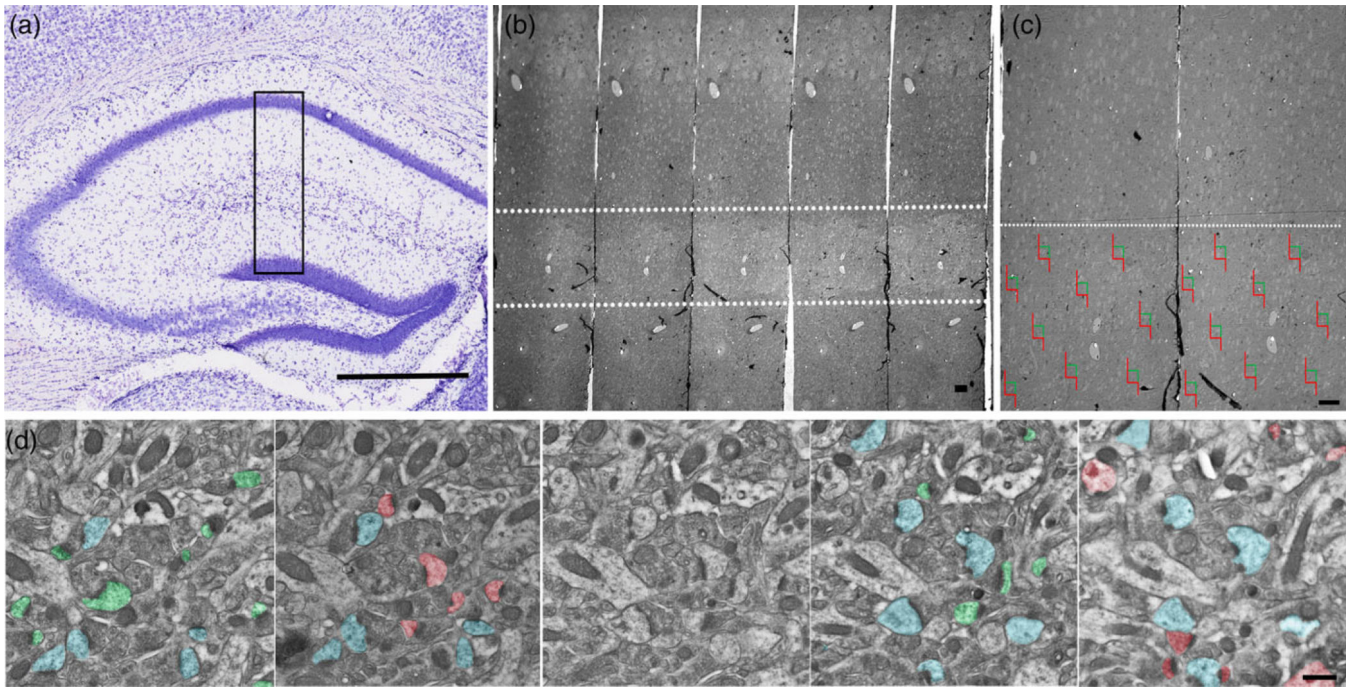

FIGURE 1.

Schematic depicting the unbiased stereological approach taken to quantify synapses. (a) EM blocks were cut encompassing mouse CA1 SR region (black box), (b) serial sections were collected and imaged between 150 and 250 μm from the cell bodies in the pyramidal layer of CA1 (white dashed lines). (c) Example of randomized imaging protocol using physical disector approach. (d) Serial electron micrographs depicting axospinous synapses counted using the disector method. Only synapses that are present in the reference panel (green and red), but not in the look-up panel was counted. Synapses present in both panels (blue) were not included in the analysis. Scale bars: a 500 μm; b 10 μm; c 10 μm; d 500 nm

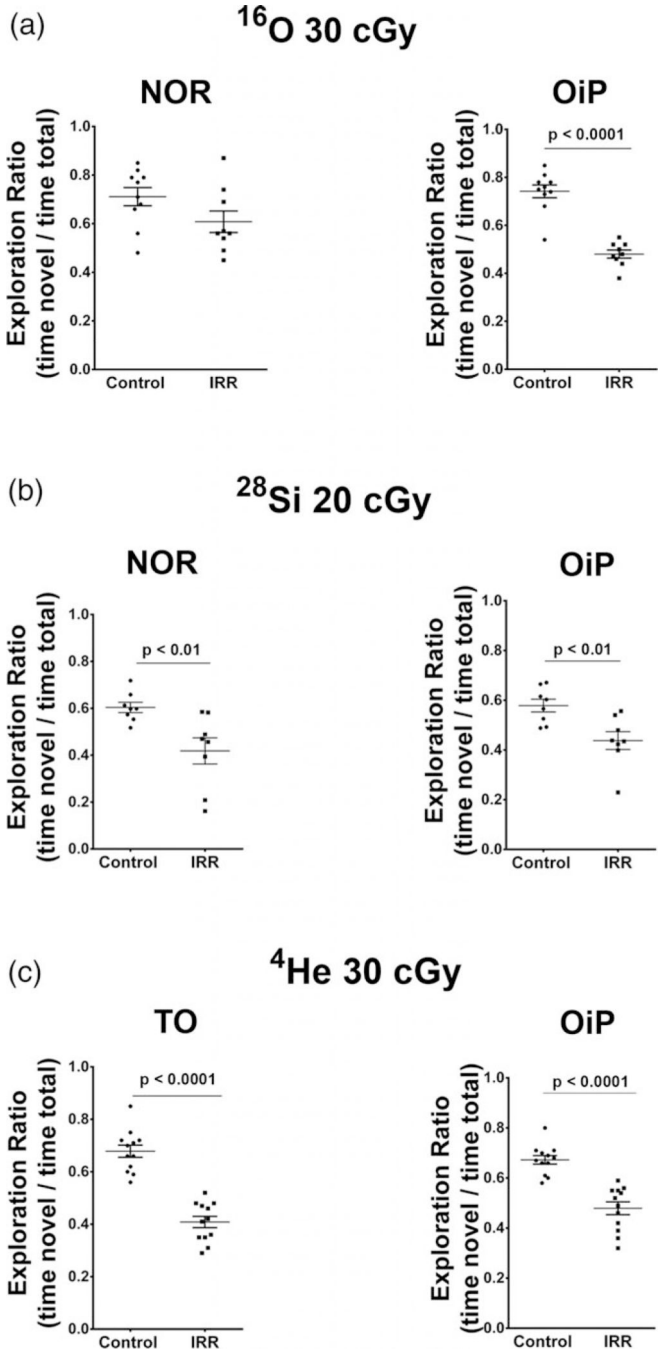

FIGURE 2.

Cognitive data adapted from previously published work reveals that similar doses of the ions used in the present study elicit significant neurobehavioral deficits 6 weeks following exposure. (a) Novel object recognition (NOR) and object in place (OiP) tasks reveal significant deficits on the OiP task after exposure to energetic ^{16}O ions (Adapted from Parihar et al., 2015a). (b) Animals subjected to similar tasks following exposure to a slightly lower dose of ^{28}Si ions exhibit significant deficits in NOR and OIP memory (Adapted from Acharya et al., 2017). (c) Animals exposed to the ^{4}He ions and subjected to the temporal

order (TO) and OiP tasks show significant impairments in each of these tasks (Adapted from Parihar et al., 2018)

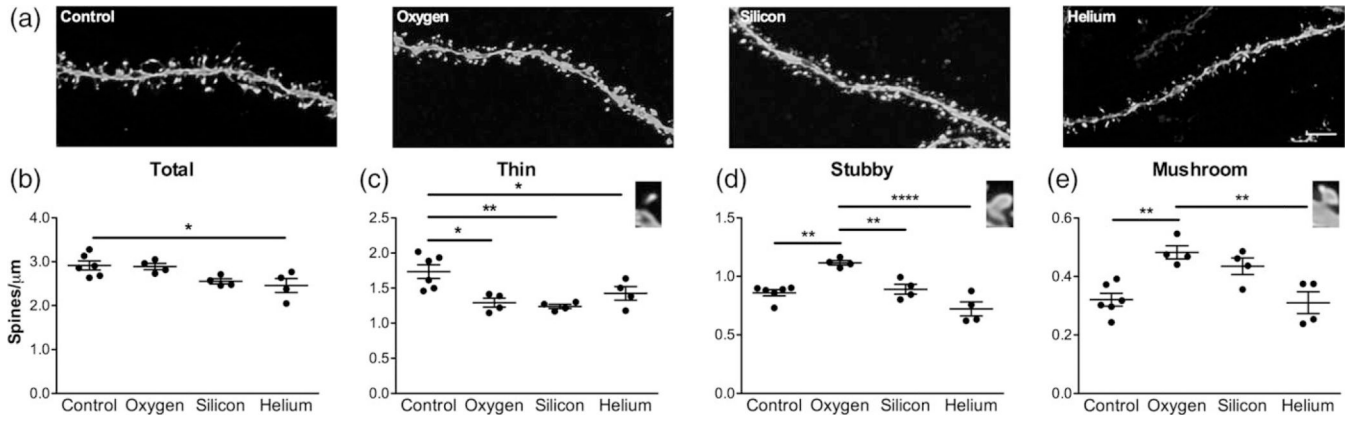

FIGURE 3.

Charged particle irradiation results in altered spine density. Analysis of spine density in CA1 apical dendritic spines revealed significant changes in spine densities on apical dendrites from CA1 pyramidal neurons. (a) Representative dendritic images from all treatment groups. Scale bar = 2 mm. (b) Average total spine density, (c) thin spine density, (d) stubby spine density and (e) mushroom spine density. Inset images in c, d and e depict each spine type. Data represent means ± SEM. One-way ANOVA *$p < 0.01$, **$p < 0.001$, ****$p < 0.0001$

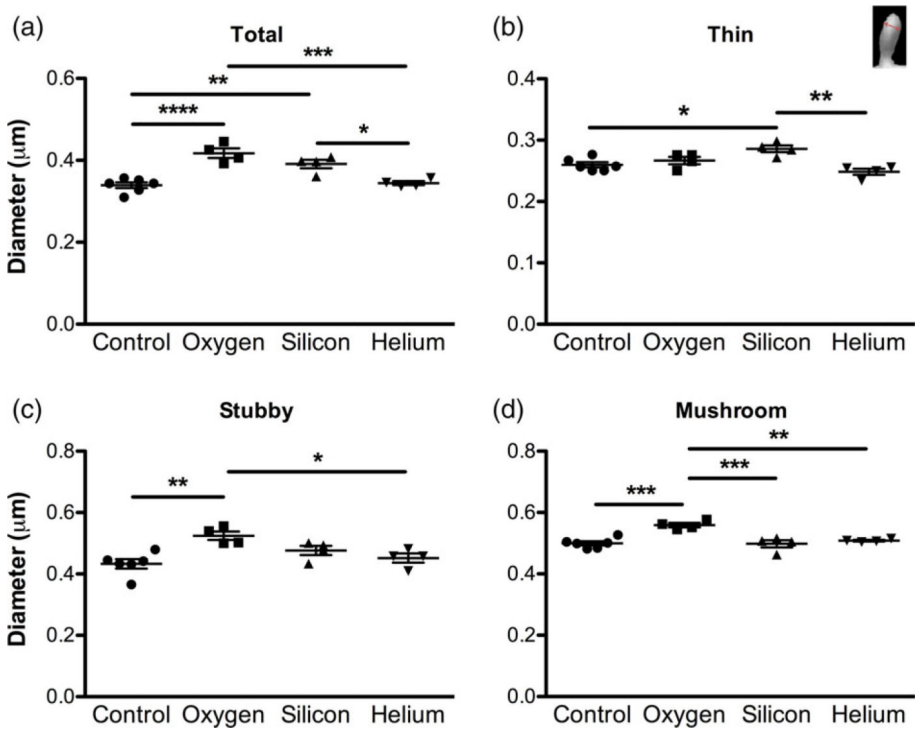

FIGURE 4.

Charged particle irradiation results in changes in spine morphology. Analysis of spine head diameter in CA1 apical dendritic spines. (a) Average total spine head diameter, (b) thin spine head diameter, (c) stubby spine head diameter and (d) mushroom spine head diameter. Inset image in b shows how spine head diameter was assessed. Data represent means ± SEM. One-way ANOVA *$p < 0.05$, **$p < 0.01$, ***$p < 0.001$, ****$p < 0.0001$ [Color figure can be viewed at wileyonlinelibrary.com]

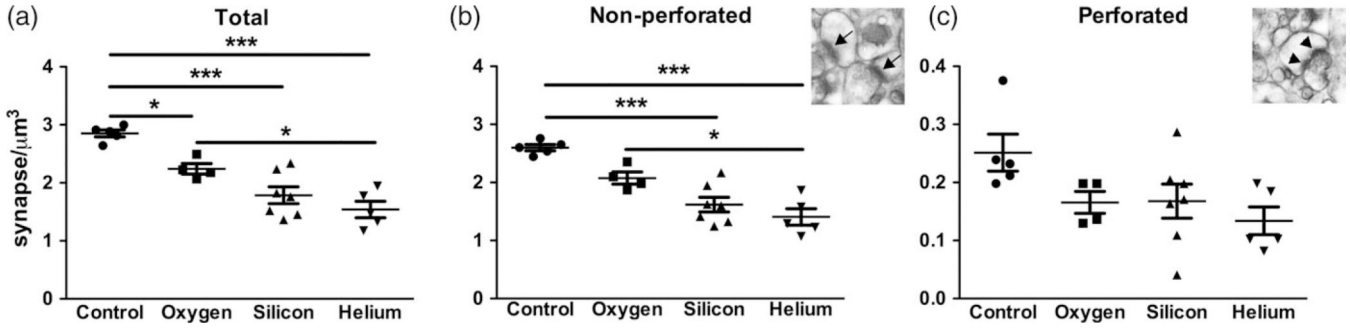

FIGURE 5.

Charged particle irradiation results in a decrease in synapse density. There is a significant decrease in total (a) and nonperforated (b) synapse density in response to irradiation with ^{16}O, ^{28}Si, and ^{4}He. No significant differences were observed in the density of perforated (c) synapses. Inset images depict nonperforated synapses (arrows), and perforated synapses (arrowheads). Data represent group means ± SEM, with each data point representing the average measurements from at least nine series images from a mouse (n = 4–7 mice/group). One-way ANOVA *$p < 0.05$, ***$p < 0.0001$

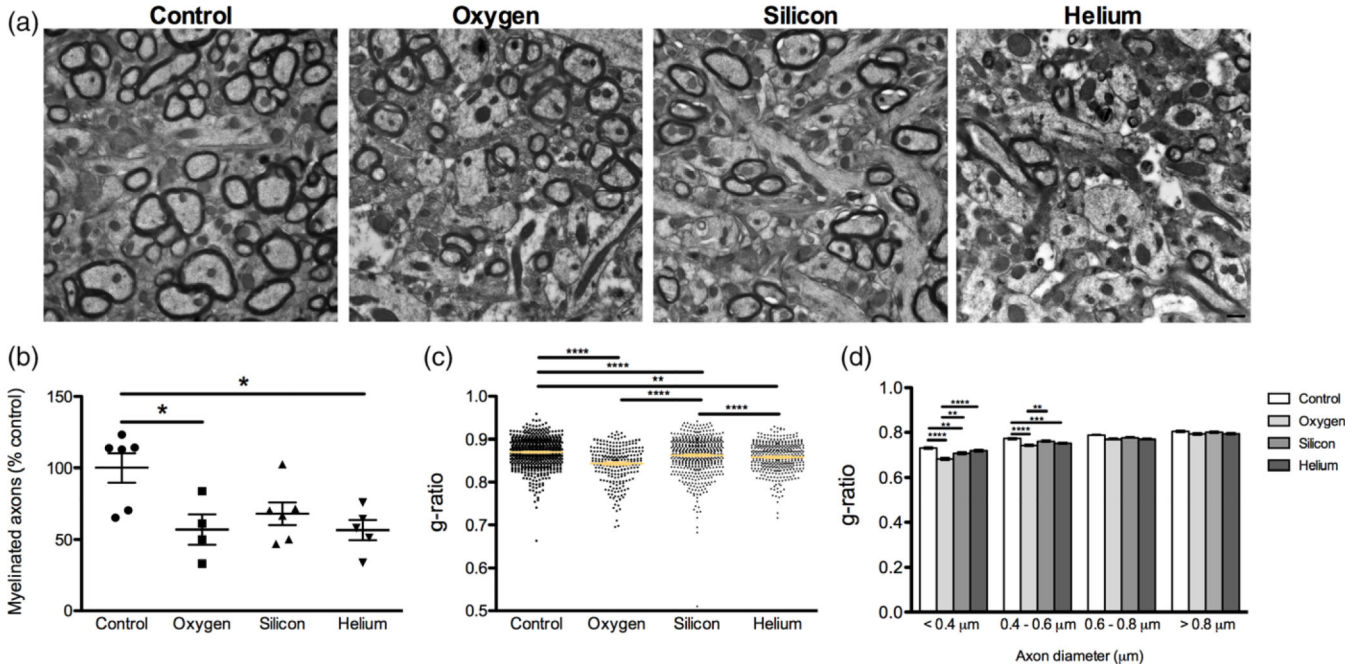

FIGURE 6.

Alterations in myelination in response to charged particle irradiation. (a) Representative myelin images from all treatment groups. Scale bar = 500 nm. (b) There was a significant decrease in the percentage of myelinated axons in ^{16}O, ^{28}Si, and ^{4}He irradiated animals compared to controls. Data represents group means ± SEM, with each data point representing the average measurements from 12 images/mouse (n = 4–7 mice/group). (c) g-ratios are lower in irradiated mice compared to controls (d) g-ratio (axon diameter/fiber diameter) of fibers grouped by axon diameter. Data represents individual measurements ± SEM, from at least six images/mouse (n = 4–7 mice/group). One-way ANOVA *$p < 0.01$, **$p < 0.001$, ***$p < 0.0001$ [Color figure can be viewed at wileyonlinelibrary.com]

Table 1.

Summary of number of animals, spines, and synapses analyzed for each group

	Control	Oxygen	Silicon	Helium	TOTAL
Spines					
Animals	5	4	4	4	17
Dendritic segments	50	42	45	42	179
Total spines	6,275	6,497	6,265	5,312	24,349
Synapses					
Animals	6	4	7	4	21
Total synapses	4,717	2,626	3,579	2,256	13,178
Axons					
Animals	6	4	7	4	21
Axons	6,862	4,935	7,764	6,490	26,051